

**Modeling of Underwater Noise
at the Bull Arm Construction Site**

Prepared in support of the:

**Hebron Project
Comprehensive Study Report**

For:

Hebron

**Suite 701, Atlantic Place
215 Water Street
St. John's, NL, A1C 6C9**

Prepared by:

JASCO Applied Sciences
Suite 432 – 1496 Lower Water Street
Halifax, NS
B3J 1R9

May 2010

HEBRON PROJECT: MODELING OF UNDERWATER NOISE AT THE BULL ARM CONSTRUCTION SITE

Version 4.0

by



Isabelle Gaboury

Terry Deveau

Mikhail Zykov

JASCO Applied Sciences

Suite 432 – 1496 Lower Water Street, Halifax, Nova Scotia B3J 1R9

Tel: +1.902.405.3336

Email: halifax@jasco.com

for

Stantec Consulting Ltd.

607 Torbay Rd., St. John's, Newfoundland A1A 1B3

Tel: +1.709.576.1458

20 September 2011

<i>Version</i>	<i>Date</i>	<i>Description</i>	<i>Approved by:</i>
1.0	15 September 2009	First draft, released to Stantec	Isabelle Gaboury
2.0	14 December 2009	Fixed error in the model results section; removed references to ANFO	Isabelle Gaboury
3.0	14 January 2010	Updated Appendix number and figure captions	Isabelle Gaboury
4.0	20 April 2010	Updated GBS base diameter; changed headers and captions to suit a stand-alone report (rather than an Appendix)	Isabelle Gaboury

Table of Contents

LIST OF TABLES	IV
LIST OF FIGURES	IV
1 INTRODUCTION.....	6
2 MODELING SCENARIOS AND SOURCE LEVEL CHARACTERIZATION	7
2.1 Impact Hammering.....	8
2.2 Vessel Traffic	9
2.3 Blasting	10
3 MODELING METHODOLOGY	13
3.1 Sound Propagation Model.....	13
3.2 Noise Metrics	14
3.2.1 Estimating 90% RMS SPL from SEL.....	15
3.2.2 M-Weighting for Marine Mammal Hearing Abilities.....	16
4 MONM PARAMETERS	18
4.1 Source Locations	18
4.2 Bathymetry and Acoustic Environment	18
4.2.1 Bathymetry.....	18
4.2.2 Geoacoustic Properties.....	19
4.2.3 Sound Speed Profiles	20
5 MODEL RESULTS	23
5.1 Impact Hammering.....	23
5.1.1 Cumulative SEL.....	26
5.2 Vessel Traffic	28
5.3 Blasting	30
6 REFERENCES.....	32
6.1 Literature Cited.....	32
6.2 Internet Sites	33

List of Tables

Table 1: Functional hearing groups of marine mammals listening underwater, and associated auditory bandwidths (from Miller <i>et al.</i> , 2005; Southall <i>et al.</i> , 2007).	17
Table 2: Locations of sites for modeling of underwater noise associated with GBS construction activities in Great Mosquito Cove and Bull Arm.....	18
Table 3: Geoacoustic model for the Great Mosquito Cove area.....	20
Table 4: Geoacoustic model for the Bull Arm area	20
Table 5: Estimated 95 th percentile radii for impact hammering at the casting basin wall in Great Mosquito Cove.....	24
Table 6: Estimated 95 th percentile radii for impact hammering at the deepwater site in Bull Arm.....	24
Table 7: Estimated 95 th percentile radii for operation of a tug at the casting basin wall in Great Mosquito Cove.....	28
Table 8: Estimated 95 th percentile radii for operation of a tug at the deepwater site in Bull Arm.....	28
Table 9: Estimated 95 th percentile radii for blasting near the exit from the casting basin in Great Mosquito Cove. The 120 dB re 1 μ Pa contour is truncated to the east for the flat and M _{lf} weightings.....	30

List of Figures

Figure 1: Locations of sites for modeling of underwater noise associated with GBS construction activities in Great Mosquito Cove and Bull Arm. Background map courtesy of Jacques Whitford Stantec Ltd. Hatched region represents the nearshore project area; dark blue circle is the deepwater GBS construction site; red circles are existing mooring points.	8
Figure 2: Third-octave band source levels for impact hammering. Source depth is 6 m above the bottom. Broad-band source level is 216 dB re 1 μ Pa @ 1 m (assuming a 10 dB SEL-to-RMS offset).....	9
Figure 3: Third-octave band source levels for a tug involved in anchor operations (a) and half-speed transit (b). Source depth is 3 m. Broad-band source levels are (a) 193 dB re μ Pa @ 1 m and (b) 185 dB re μ Pa @ 1 m. Note that only the source levels associated with anchor operations (a) were used for sound propagation modeling.	10
Figure 4: Sample CONWEP output, for 2 kg of TNT buried at 7.1 m depth in rock, and a receiver placed 20 m away at the same burial depth as the source	11
Figure 5: Equivalent third-octave band source levels for detonation of 2 kg of TNT at a burial depth of 7.1 m. Broadband source level is 231 dB re 1 μ Pa @ 1 m.	12
Figure 6: Plot of standard M-weighting curves for low frequency, mid-frequency and high frequency cetaceans, and for pinnipeds in water (from Southall <i>et al.</i> , 2007).....	17
Figure 7: Model sites and depth contours for the Bull Arm model area.....	19
Figure 8: Typical monthly sound speed profiles in SW Trinity Bay, based on GDEM	21
Figure 9: Average February and September sound speed profiles at 47.75°N, 53.75°W, based on GDEM	22

Figure 10: Estimated un-weighted, single-blow sound pressure level for operation of an impact hammer at the casting basin wall in Great Mosquito Cove (top panel) and at the deepwater site (bottom panel). Modeled source depth is 6 m above the sea floor in both cases..... 25

Figure 11: Estimated 198 dB re 1 $\mu\text{Pa}^2\cdot\text{s}$ cumulative SEL contour for impact hammering at the casting basin wall, assuming a blow rate of 32 blows/minute and CSEL integration periods from 1 minute to 24 hours. Contours are shown for low-frequency (top panel) and high-frequency (bottom panel) cetacean M-weightings. Setup otherwise as in the upper panel of Figure 10. 27

Figure 12: Estimated un-weighted sound pressure level for operation of a tug at the casting basin wall in Great Mosquito Cove (top panel) and at the deepwater site (bottom panel). Source depth is 3 m in both cases. 29

Figure 13: Estimated un-weighted, single-blast sound pressure level for detonation of 2 kg of TNT 7.1 m sub-bottom near the exit from the casting basin in Great Mosquito Cove. The 120 dB re 1 μPa contour is truncated to the east as a result of the model bounds used..... 31

1 Introduction

As part of the development of the Hebron Project, ExxonMobil has proposed to set up and operate an onshore/nearshore construction area in Bull Arm, located in Trinity Bay, Newfoundland and Labrador. The construction area is to be used for Gravity Based Structure (GBS) construction, topsides assembly, and installation of the topsides onto the GBS before tow-out of the completed platform to the offshore area in The Jeanne d'Arc sedimentary basin, off the east coast of Canada. Construction of the GBS base slab and lower caisson walls will take place in Great Mosquito Cove, a small bay within Bull Arm. Topside portions of the platform will be constructed at a location on the northern shore of Great Mosquito Cove, for mating with the GBS at a deepwater site in Bull Arm.

Underwater noise will be generated during a variety of activities occurring during construction of the GBS and topsides, and may impact the marine environment to varying degrees. For instance, blasting and impact hammering are relatively loud, but short in duration. Vessel traffic generates much lower levels of noise, but will occur over a greater portion of the overall construction process.

A modeling study has been carried out to determine the levels of underwater sound resulting from blasting, impact hammering, and vessel traffic during construction of the GBS. The acoustic model produces *a priori* estimates of the anticipated sound field generated by these activities. The model accounts for source characteristics and acoustic propagation in a complex, multi-layered, non-homogeneous ocean environment. This approach takes into account the specific properties of the water column and bottom in the area of operation, insofar as they are known.

Scenarios modeled as part of this study are described in Section 2, as are the activity-specific source levels input to the sound propagation model. Model methodology is outlined in Section 3. Section 4 describes the source location and modeling parameters required by the propagation model. Finally, the results of the modeling study are discussed in Section 5.

2 Modeling Scenarios and Source Level Characterization

While any in-water or near-shore activities occurring during construction of the Gravity Based Structure (GBS) have the potential to introduce noise into the underwater environment, three activities were identified as being particularly important in terms of their potential impacts:

1. Impact hammering associated with placement of the sheet piles to enclose the casting basin in Great Mosquito and with installation of moorings at the deepwater site in Bull Arm
2. Vessel traffic associated with construction activities in both Great Mosquito Cove and Bull Arm
3. Blasting, which may occur if the final design of the GBS is such that the channel leading from the casting basin into Great Mosquito Cove must be widened

The corresponding locations used for modeling are shown in Figure 1 below, and discussed further in Section 4.1. Impact hammering and blasting will likely be the loudest of those involved in construction of the GBS. Vessel traffic generates much lower levels of underwater noise, but will occur during a much longer period of time.

At the time of writing of this document, the specific equipment associated with each of these activities had not yet been identified. As such, sample model scenarios were constructed based on “typical” equipment that might be used for a given activity, using existing measurements or models; source levels for each activity are discussed in the sub-sections below. Source levels can vary considerably for a given activity, depending on the specific equipment used and how it is operated. Wherever it was appropriate to do so, louder sources were selected for the model scenarios, so that the resulting underwater sound estimates (presented in Section 5) are likely to be similar to or higher than those actually generated during construction of the GBS. However, actual levels of underwater sound generated during GBS construction could be higher if a particularly loud piece of equipment is used (e.g., larger impact hammer or tug).

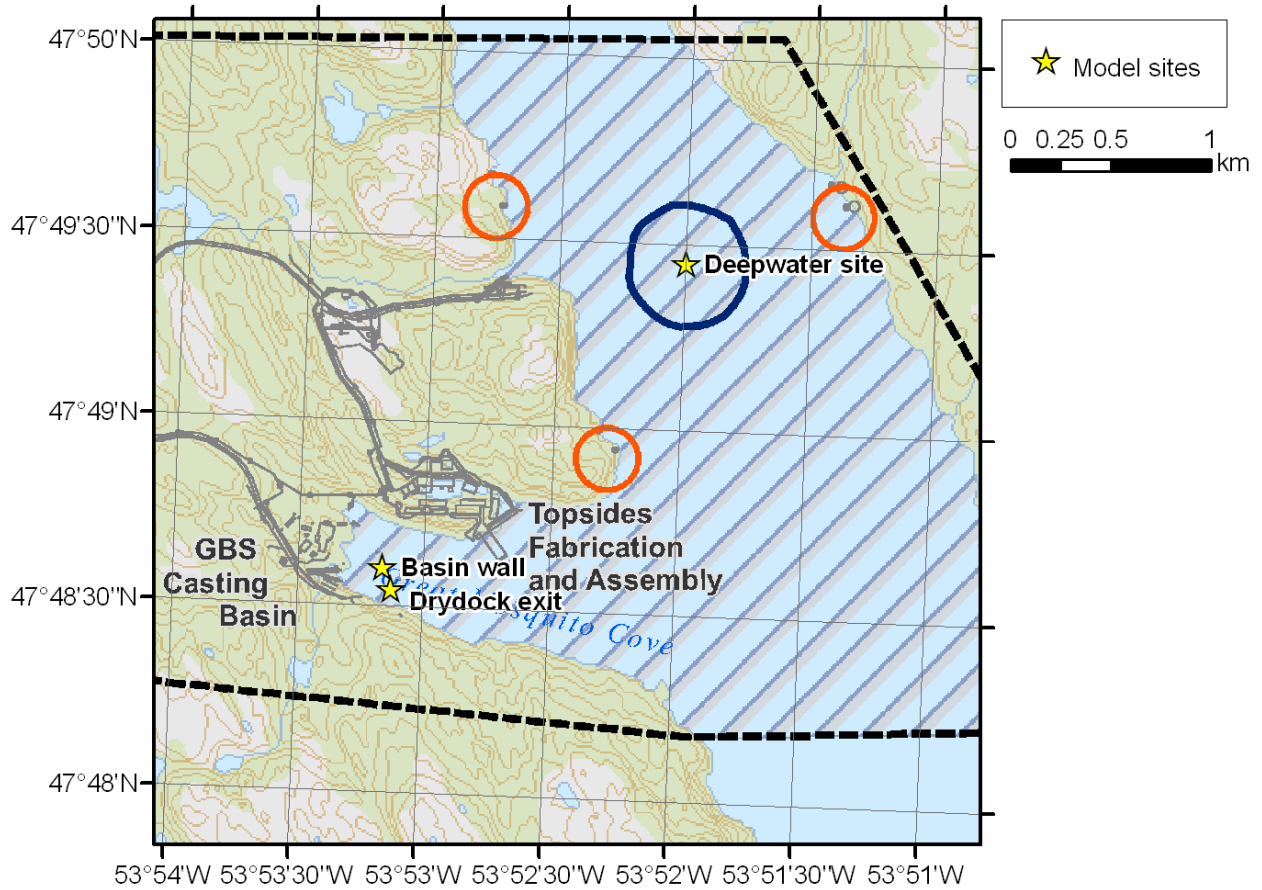


Figure 1: Locations of sites for modeling of underwater noise associated with GBS construction activities in Great Mosquito Cove and Bull Arm. Background map courtesy of Jacques Whitford Stantec Ltd. Hatched region represents the nearshore project area; dark blue circle is the deepwater GBS construction site; red circles are existing mooring points.

2.1 Impact Hammering

Impact hammering may be required to complete installation of the sheet piles during construction of the GBS casting basin and for mooring installation at the deepwater site (Figure 1). Source levels for impact hammering at both sites were based on a Menck MHU 3000 hydraulic hammer, which is capable of operating in waters up to 400 m (Menck GmbH, 2009). This is a relatively large impact hammer, with impact energy ranging from 300 to 3050 kJ/blow. Source levels were based on measurements presented by Greene and Davis (1999), for pile driving on the Scotian Shelf. The broadband source exposure level was calculated by Malme *et al.* (1998) to be 205.9 dB re 1 $\mu\text{Pa}^2\cdot\text{s}$. Root-mean-square source levels in dB re 1 μPa @ 1m were estimated assuming a pulse length of 100ms, using the following formula (see also Section 3.2.1):

$$\text{SPL}_{\text{RMS}} \text{ (dB re 1 } \mu\text{Pa@1m)} = \text{SEL (dB re 1 } \mu\text{Pa}^2\cdot\text{s)} - 10 \text{ Log T, where T = 100ms,}$$

under the assumption that all sound energy is received in a 100 ms time window. In this case the 10 log T term is equal to 10 dB, giving the result that SPL_{RMS} is numerically equal to $\text{SEL} + 10 \text{ dB}$. The resulting 1/3 octave band energy levels are shown in Figure 2.

For pile driving at the casting basin, the source depth was set to approximately half the local water depth, i.e. 6 m. In actuality, sound will radiate from all portions of the pilings; this mid-water column value is a precautionary estimate of the depth for an equivalent point source, as losses due to

bottom and surface interactions will be less for a source at mid-depth than for one near the sea floor or surface. Because the length of the piling to be installed at the deepwater site is not known, the same height above the sea floor was used as for the casting basin site (6 m above the bottom, or a source depth of approximately 124 m).

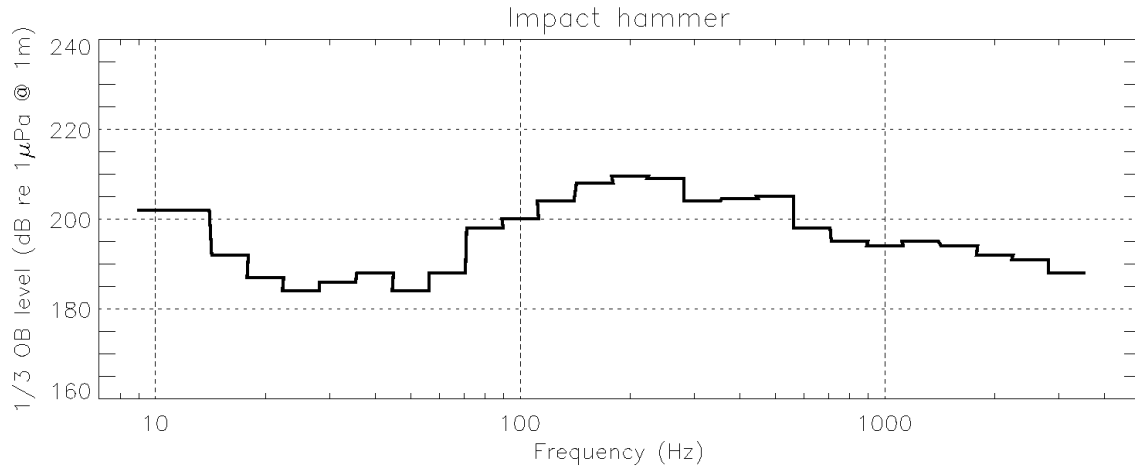


Figure 2: Third-octave band source levels for impact hammering. Source depth is 6 m above the bottom. Broad-band source level is 216 dB re 1 μ Pa @ 1 m (assuming a 10 dB SEL-to-RMS offset).

2.2 Vessel Traffic

Working tugs are generally amongst the loudest of the vessel sources present at a construction site. For the current model scenario, source levels were based on a relatively large tug, the Britoil 51 (Britoil Offshore Services Website). The Britoil 51 has a main propulsion power of 6600 bhp, supplemented by a 500 bhp bow-thruster. Measured 1/3 octave band source levels for the Britoil 51 are shown in Figure 3 for anchor pulling operations (i.e., operating near full power) and for transit at half speed (Hannay *et al.*, 2004). Because the tug is much louder during high-power operations (e.g., pushing/pulling or transit at full speed), the source levels associated with anchor pulling (Figure 3(a)) were used for the model runs. Source depth was taken to be approximately half the vessel’s draught, i.e. 3 m, based on the reasonable assumption that the majority of the underwater sound generated by the vessel will be associated with propeller cavitation.

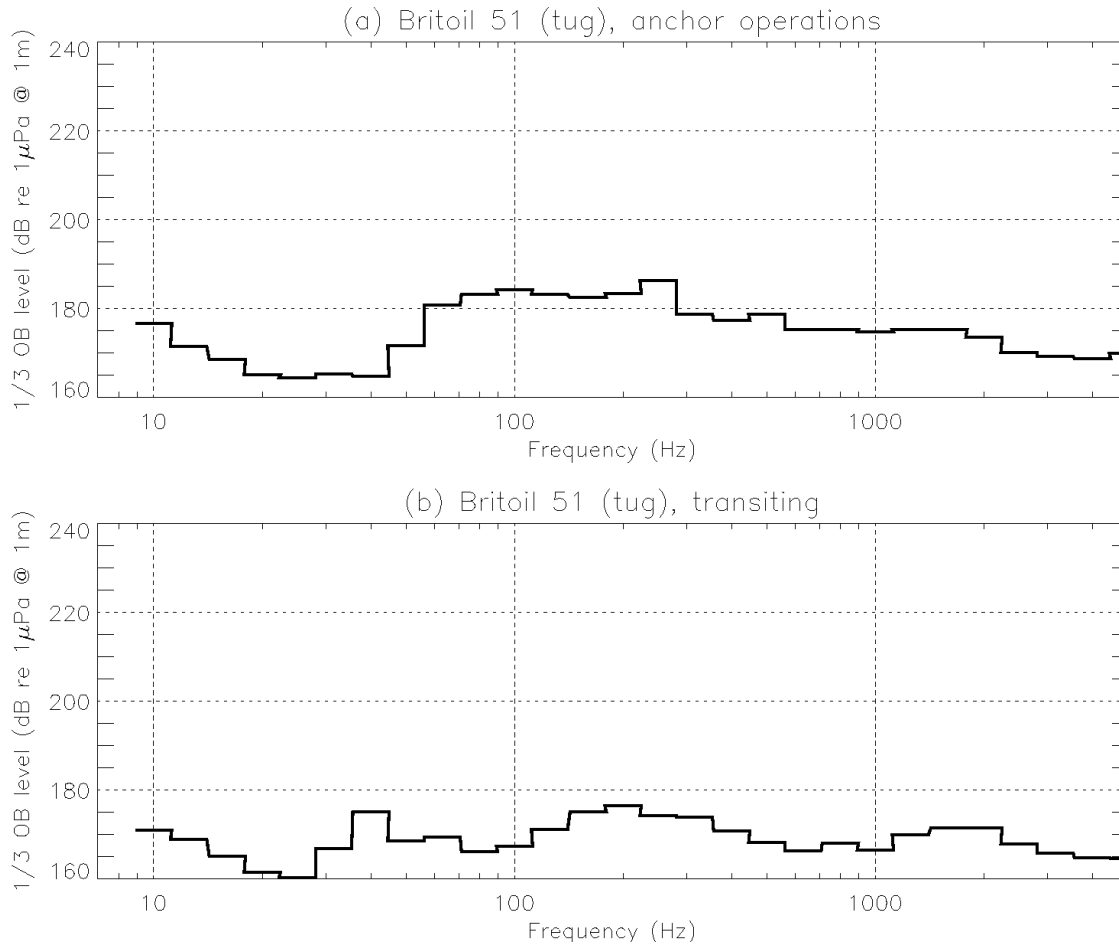


Figure 3: Third-octave band source levels for a tug involved in anchor operations (a) and half-speed transit (b). Source depth is 3 m. Broad-band source levels are (a) 193 dB re μPa @ 1 m and (b) 185 dB re μPa @ 1 m. Note that only the source levels associated with anchor operations (a) were used for sound propagation modeling.

2.3 Blasting

As of the time of writing of this document, the design for the GBS called for a base slab diameter of 125-135 m and a draught of 16 m when leaving the casting basin. Based on these dimensions (which may decrease during the final design stages), some sub-tidal blasting will be required near the exit from the GBS casting basin in order to widen the channel for tow-out.

Because the details of the potential blasting have not yet been determined, a sample scenario was constructed using the simple case of a single explosive charge with size and burial depth as prescribed by current DFO guidelines, which state that the instantaneous pressure change in or near fish habitat is not to exceed 100 kPa (Wright and Hopky, 1998). Based on the presence of shallow bedrock in Great Mosquito Cove (Section 4.2.2) and possible combinations of charge weight and burial depth outlined in Table 1 of Wright and Hopky (1998), a TNT equivalent charge weight of 2 kg was used for source modeling, with a burial depth of 7.1 m (assuming rock as the substrate).

Detonation of a buried explosive generates an in-ground pressure shock wave, which propagates through the substrate and into the water column. The blast effects model CONWEP (Hyde, 1992) can be used to predict the shape of the in-ground shock wave pressure at distance from the detonation site. The output from CONWEP is a history of pressure as a function of time at some distance from the source for a

given explosive type and weight, source-receiver geometry, and substrate. For instance, Figure 4 shows the waveform output by CONWEP for detonation of 2 kg of TNT buried at a depth of 7.1 m in rock and for a receiver placed at a distance of 20 m from the source at the same burial depth. Note that the peak pressure shown in this figure is considerably higher than the peak pressure that would be experienced in water at this range, as energy is lost during transmission from the sub-bottom into the water column.

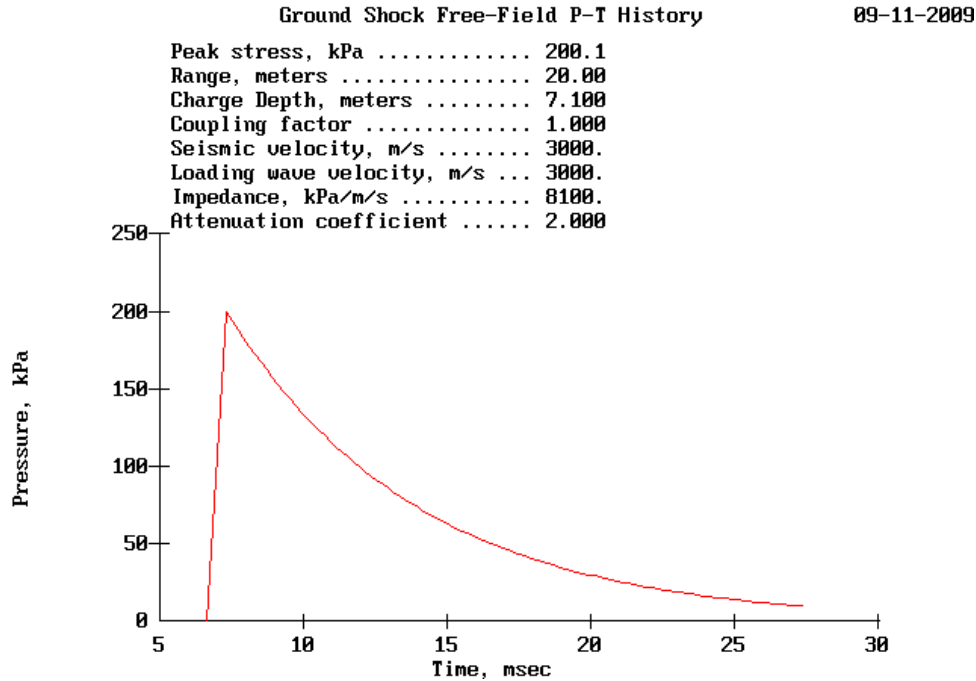


Figure 4: Sample CONWEP output, for 2 kg of TNT buried at 7.1 m depth in rock, and a receiver placed 20 m away at the same burial depth as the source

Because the physics of explosive detonation are complex in the immediate vicinity of the blast, a blast effects model such as CONWEP cannot be used to directly yield sound levels at or very near the source. Instead, CONWEP was run for a range well outside the non-linear region near the detonation, and the equivalent third-octave band source levels (similar to those presented in the preceding sections) were back-propagated using a sound propagation model. This was done as follows:

1. CONWEP was run using the explosive setup and geometry described above, for a horizontal range of 20 m. The output is the waveform shown in Figure 4.
2. Third-octave band SPL's at a range of 20 m were computed by taking the Fourier transform of the pressure history shown in Figure 4 and filtering into third-octave bands.
3. The sound propagation model RAM (discussed in Section 3.1) was used to compute the transmission loss in each third-octave band, to a maximum range of 20 m for a receiver in the seabed. The setup used for RAM was identical to that used for the main sound propagation modeling (see Sections 3 and 4), with the exception that a flat bottom with a depth of 12 m (the local bottom depth at the site used for modeling of the full sound field) was used.
4. The third-octave band transmission losses computed in step 3 were added to the SPLs computed in step 2 to yield equivalent third-octave band source levels (see Section 3).

The result of these computations is shown in Figure 5 below. Note that these are not the actual levels that would be measured at the detonation site; rather, they represent “equivalent” source levels, which when forward-propagated in a realistic acoustic environment (as outlined in Section 3.1) yield the same received levels at a horizontal range of 20 m as would be predicted using CONWEP.

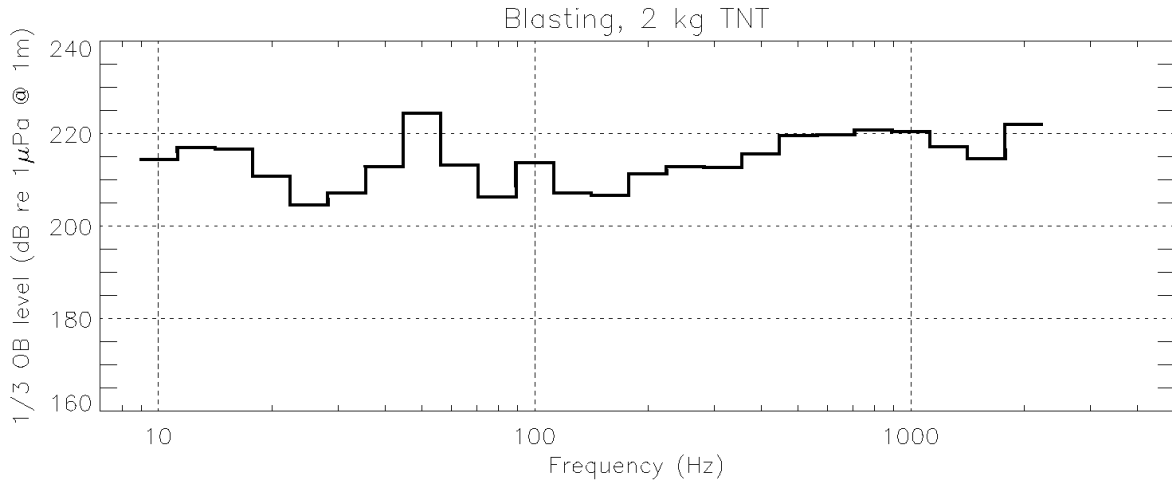


Figure 5: Equivalent third-octave band source levels for detonation of 2 kg of TNT at a burial depth of 7.1 m. Broadband source level is 231 dB re 1 μPa @ 1 m.

3 Modeling Methodology

Starting from the source location and levels for a given scenario (Section 2), the acoustic field at any range from the source is estimated using an acoustic propagation model. Sound propagation modeling uses acoustic parameters appropriate for the specific geographic region of interest, including the expected water column sound speed profile, the bathymetry, and the bottom geoacoustic properties, to produce site-specific estimates of the radiated noise field as a function of range and depth. MONM, described in section 3.1, is used to predict the directional transmission loss footprint from source locations corresponding to trial sites for experimental measurements. The received level (RL) at any 3-dimensional location away from the source is calculated by combining the source level (SL) and transmission loss (TL), both of which are direction dependent, using the following relation:

$$RL = SL - TL$$

Acoustic transmission loss and received sound levels are a function of depth, range, bearing, and environmental properties. In the case of impulsive sources such as explosives or impact hammering, the received levels estimated by MONM, like the source levels from which they are computed, are expressed as the sound exposure level (SEL). SEL is expressed in units of dB re $1\mu\text{Pa}^2 \cdot \text{s}$ and is a measure related to the acoustic energy in a single pulse (blast or hammer blow). In the case of continuous sources such as vessel noise, the SEL received in 1 second is equivalent to the RMS sound pressure level (SPL). In both cases, the values output by MONM may be used to compute or estimate specific noise metrics relevant to safety and disturbance criteria, a process which may involve filtering for frequency-dependent marine mammal hearing capabilities. This is discussed in Section 3.2.

3.1 Sound Propagation Model

Source levels (discussed in Section 2) are used as input for the acoustic propagation software MONM (Marine Operations Noise Model), which computes the sound field as a function of range, depth, and bearing relative to the source location. MONM, a proprietary application developed by JASCO Applied Sciences, is an advanced modeling package whose algorithmic engine is a modified version of the widely-used Range Dependent Acoustic Model, RAM (Collins *et al.*, 1996).

RAM is based on the parabolic equation method using the split-step Padé algorithm to efficiently solve range-dependent acoustic problems. RAM assumes that outgoing energy dominates over scattered energy, and computes the solution for the outgoing wave equation. An uncoupled azimuthal approximation is used to provide two-dimensional transmission loss values in range and depth, i.e., computation of the transmission loss as a function of range and depth within a given radial plane is carried out independently of neighboring radials (reflecting the assumption that sound propagation is predominantly away from the source). RAM has been enhanced by JASCO to model (to a first approximation) shear wave conversion at the sea floor; the model uses the equivalent fluid complex density approach of Zhang and Tindle (1995). For reflection from the sea-surface, it is assumed that the surface is smooth (i.e., reflection coefficient with a magnitude of -1). While a rough sea surface would increase scattering (and hence transmission loss) at higher frequencies, the scale of surface roughness is insufficient to have a significant effect on sound propagation at the lower frequencies where most of the energy of the sources described in Section 2 occurs, particularly at the shallower grazing angles that are most important to horizontal propagation.

Because the modeling takes place over radial planes in range and depth, volume coverage is achieved by creating a fan of radials sufficiently dense to provide the desired tangential resolution. This $n \times 2-D$ approach can be modified in MONM to achieve greater computational efficiency by not over-sampling the region close to the source, obtaining the desired coverage through a process of tessellation. The tessellation algorithm also allows the truncation of radials along the edges of a bounding quadrangle of arbitrary shape, further contributing to computational efficiency by enabling the modeling region to be

more closely tailored to an area of relevance. MONM has the capability of modeling sound propagation from multiple directional sources at different locations and merging their acoustic fields into an overall received level at any given location and depth. This feature was not required in the present study.

The received sound levels at any location within the region of interest are computed from the $\frac{1}{3}$ -octave band source levels by subtracting the numerically modeled transmission loss at each $\frac{1}{3}$ -octave band center frequency, and summing across all frequencies to obtain a broadband value. For this study, transmission loss and received levels were modeled for $\frac{1}{3}$ -octave frequency bands between 10 and 2000 Hz. Because the sources of underwater noise considered in this study are predominantly low-frequency sources (see Sections 2), this frequency range is sufficient to capture essentially all of the energy output by these activities. The received levels, like the source levels from which they are computed, are equivalent to sound exposure level (SEL) (see Section 3.2 below). In the case of continuous sources they are equivalent to SEL over 1 second, or equivalently SPL.

3.2 Noise Metrics

By convention, noise underwater is measured in decibels relative to a fixed reference pressure of 1 μPa . However, the loudness and biological effects of impulsive noise (e.g., from pile driving) are not, in general, proportional to instantaneous acoustic pressure and so several different sound level metrics (i.e., different ways of quantifying sound level) are commonly used. The three most commonly employed sound level metrics found in the literature are peak sound pressure level (PSPL), root mean square (RMS) sound pressure level (SPL) and sound exposure level (SEL).

The peak sound pressure level (symbol L_{pk}) is the maximum instantaneous sound pressure level attained by an impulse, $p(t)$:

$$L_{pk} = 20 \log_{10} (\max |p(t)|)$$

The RMS sound pressure level or SPL (symbol L_p) is the mean square pressure level over a time window, T , containing the impulse:

$$L_p = 10 \log_{10} \left(\frac{1}{T} \int_T p^2(t) dt \right)$$

For impulsive sources this is typically much less than the peak pressure. By convention, when computing safety radii the time interval, T , is most often taken to be the “90% energy pulse duration” rather than over a fixed time window (Malme *et al.*, 1986; Greene, 1997; McCauley *et al.*, 1998); the time window, T_{90} , is computed for each pulse as the interval containing 90% of the pulse energy — this is commonly referred to as the 90% RMS SPL (American National Standards Institute (ANSI) symbol L_{p90}). Because the window length, T , is used as a divisor, pulses that are more spread out in time have a lower RMS level for the same total acoustic energy.

The sound exposure level or SEL (ANSI symbol L_E) is the time-integral of the square pressure over a fixed time window long enough to include the entire pulse:

$$L_E = 10 \log_{10} \left(\int_T p^2(t) dt \right) = L_p - 10 \log_{10}(T)$$

Comparing this expression with the above definition of L_p , the only difference is the lack of the $1/T$ divisor, as SEL is an integral rather than an average; i.e., L_p is numerically equal to L_E computed over a 1 second time window for a signal with a constant intensity over the time window. SEL has units of dB re $\mu\text{Pa}\cdot\sqrt{\text{s}}$ or equivalently dB re $\mu\text{Pa}^2\cdot\text{s}$. It is a measure of sound energy (or exposure) rather than sound pressure. Unless stated otherwise, SELs presented in this report represent sound exposure from single pulses. For a multiple-pulse source such as an impact hammer, multiple exposures may be summed to

produce a single exposure “equivalent” value if one makes the precautionary assumption that the inter-pulse interval is too short for recovery from any noise-induced hearing impairment (Southall *et al.*, 2007). In that case, the cumulative SEL (CSEL) is defined as follows:

$$\text{CSEL} = 10 \log_{10} \left\{ \frac{\sum_{n=1}^N \int_0^T p_n^2(t) dt}{p_{ref}^2} \right\}$$

Here N is the number of pulse exposures, and $p_{ref} = 1 \mu\text{Pa}$ in water.

3.2.1 Estimating 90% RMS SPL from SEL

Some of the literature on bioacoustic impact on marine animals uses the RMS sound pressure level metric, described above. For example, the U.S. National Marine Fisheries Service (NMFS) has generally required that safety and assumed “disturbance” radii around sound sources be established based on the RMS sound pressure level metric. With impulsive sources, cetaceans are not to be exposed to received levels exceeding 180 dB re $1\mu\text{Pa}_{\text{RMS}}$. Also, NMFS considers that marine mammals exposed to pulsed sounds with received levels ≥ 160 dB re $1\mu\text{Pa}_{\text{RMS}}$ may be disturbed appreciably. Sound models generally produce more stable estimates of SEL than of RMS levels, and consequently a method is required to numerically convert modeled SEL levels to RMS SPL.

As discussed above, the pulse duration for computation of RMS SPL is conventionally taken to be the interval during which 90% of the pulse energy is received. Although it is relatively straightforward to compute the 90% RMS SPL from measured sound data, this metric is difficult to model because of inherent variability of the integration period. This period is highly sensitive to the specific multipath arrival pattern from an acoustic source and can vary abruptly with distance from the source or with depth of the receiver (see expanded discussion below). To accurately predict the 90% RMS level, it is necessary to use full-waveform acoustic models. Those models are computationally intensive for range-dependent environments. The alternative and more approximate method used here involves applying a translation factor to modeled SEL values.

For both measured and modeled sound levels, the RMS metric is often unstable over space and time because the signal duration is strongly influenced by scattering and bottom-reflected energy that vary rapidly with distance from the source. This variability generally becomes larger at greater ranges from the source because of the increased effects of multiple bottom reflections on the pulse length. As a result, it becomes difficult to objectively define the 90% integration time window at longer ranges where the length of this window depends on the presence and signal strength of multiple-reflected paths. A simple example that demonstrates this problem is the deepwater case where a bottom reflection can arrive more than a second after the direct path signal. If that reflection is strong enough to account for more than 5% of the overall pulse energy, then the time window will include both the direct path and reflection, causing it to be more than 1 second in duration. A slightly weaker bottom reflection would not extend the window, and the pulse length could be on the order of tens of milliseconds. The resulting difference in RMS level for the two cases can easily be more than 15 dB, and the transition can occur abruptly as receiver distance from the source increases.

Accurate estimates of safety and disturbance ranges must take into account the acoustic energy that is returned to the water column by bottom and surface reflections. This is especially important in the case of shallow water. If multipath reflections were taken into account, the resultant temporal spreading of the received seismic pulse would change the received pulse duration, RMS estimates, and predicted radii. The MONM algorithm does not attempt to predict the RMS pressure directly; rather it models the

propagation of acoustic energy in 1/3-octave bands in a realistic, range-dependent acoustic environment. When these 1/3-octave band levels are summed, the result is a broadband Sound Exposure Level (SEL), equivalent to the sound pressure level that would occur if the energy for a single pulse were spread evenly over a nominal time window of 1 s.

From these predicted SEL values, the approximate RMS equivalents can be obtained taking into account the interrelationships of SEL, RMS level, and pulse duration as known from theory and from several empirical studies where these parameters have all been measured for the same received pulses. As outlined in the above definition of these metrics, SPL is related to SEL via a simple function that depends only on the RMS integration period T :

$$\text{SPL}_{\text{RMS90}} = \text{SEL} - 10 \log(T) - 0.458$$

Here the last term accounts for the fact that only 90% of the acoustic pulse energy is delivered over the standard integration period used for computation of $\text{SPL}_{\text{RMS90}}$. In the absence of *in situ* measurements, the integration period is difficult to predict with any reasonable degree of accuracy. In this case, a heuristic value of T , based on field measurements in similar environments, may be used to estimate an RMS level from the modeled SEL. Radii estimated in this way are approximate since the true time spreading of the pulse has not actually been modeled. For this study, the integration period T has been assumed equal to a pulse width of ~0.1 s, resulting in the following approximate relationship between RMS SPL and SEL:

$$\text{SPL}_{\text{RMS90}} = \text{SEL} + 10$$

In various studies where the $\text{SPL}_{\text{RMS90}}$, SEL, and duration have been measured empirically, the average offset between SPL and SEL has been found to be 5–15 dB, with considerable variation depending on distance from source, water depth and geo-acoustic environment (Greene, 1997; McCauley *et al.*, 2000; Austin *et al.*, 2003; Blackwell *et al.*, 2007; MacGillivray *et al.*, 2007). On average, the measured SPL–SEL offsets tend to be larger at close distances, where the pulse duration is short ($\ll 1$ s), and to diminish at longer distances, where pulse duration tends to increase because of propagation effects. As such, the use of a fixed 10 dB offset may be considered to be conservative at long ranges (i.e., the actual offset may be smaller), and the RMS SPL may be overestimated. The opposite may occur at close distances.

3.2.2 M-Weighting for Marine Mammal Hearing Abilities

In order to take into account the differential hearing capabilities of various groups of marine mammals, the M-weighting frequency weighting approach described by Miller *et al.* (2005) and Southall *et al.* (2007) is being applied increasingly commonly. The M-weighting filtering process is similar to the C-weighting method that is used for assessing impacts of strong impulsive sounds on humans. It accounts for the reduced auditory effect of sound frequencies extending above and below the most sensitive hearing range of marine mammals within each of five functional groups: low frequency cetaceans, mid-frequency cetaceans, high frequency cetaceans, and pinnipeds in water (Table 1 and Figure 6), as well as pinnipeds in air. The filter weights Mw_i , for frequency band i with center frequency f_i , are defined by

$$Mw_i = 20 \log_{10} \left(\frac{f_i^2 f_{hi}^2}{(f_i^2 + f_{lo}^2)(f_i^2 + f_{hi}^2)} \right)$$

Here f_{lo} and f_{hi} are as listed in Table 1.

Table 1: Functional hearing groups of marine mammals listening underwater, and associated auditory bandwidths (from Miller *et al.*, 2005; Southall *et al.*, 2007).

Functional hearing group	Members	Estimated functional auditory bandwidth (Hz)	
		f_{lo}	f_{hi}
Low-frequency cetaceans	Mysticetes	7 Hz	22 kHz
Mid-frequency cetaceans	Lower-frequency odontocetes	150 Hz	160 kHz
High-frequency cetaceans	Higher-frequency odontocetes	200 Hz	180 kHz
Pinnipeds (in water)	Pinnipeds	75 Hz	75 kHz

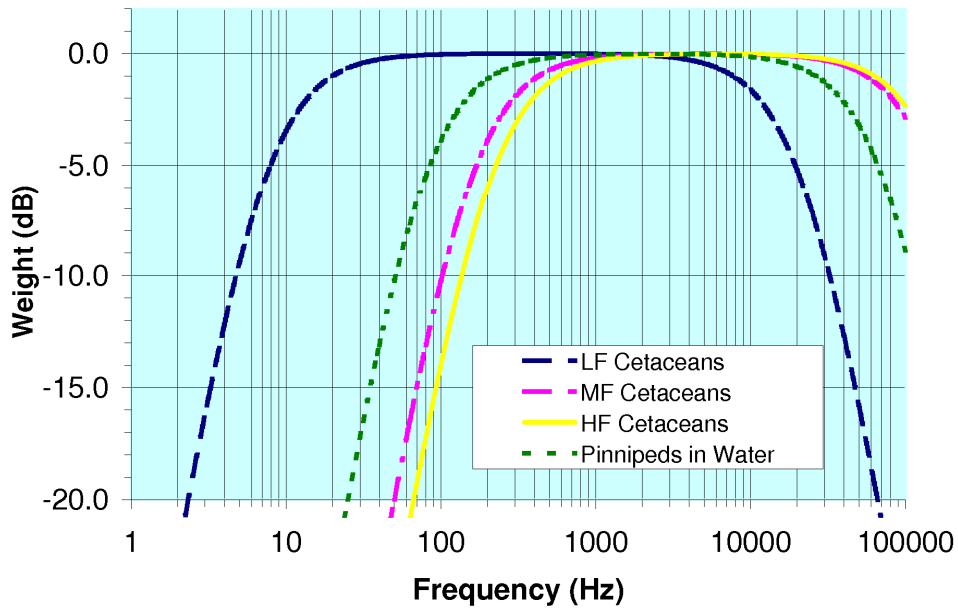


Figure 6: Plot of standard M-weighting curves for low frequency, mid-frequency and high frequency cetaceans, and for pinnipeds in water (from Southall *et al.*, 2007).

4 MONM Parameters

4.1 Source Locations

Sound propagation modeling was carried out for each of the sites shown in Table 2 below and in Figure 1 of Section 2. Source depths depended on the activity being modeled, as tabulated in Table 2 and discussed in Section 2.

From the chosen source position, the sound propagation model generates a grid of acoustic levels over any desired area and for specified receiver depths. The following receiver depths were used:

2, 4, 6, 8, 10, 12, 14, 16, 18, 20, 25, 30, 35, 40, 45, 50, 60, 70, 80, 90, 100, 125, 150, 200, 250, 300 m

This set of receiver depths samples the full range of water depths over the model area, with increased resolution near source depth. For the purposes of generating maps and tables of noise level contours, the modeled acoustic field at each x,y point was typically maximized over all receiver depths down to the local bottom depth. Maximizing received level over depth ensures that the predicted radii represent the largest possible (and therefore most precautionary) distance to any given SEL or SPL threshold.

Table 2: Locations of sites for modeling of underwater noise associated with GBS construction activities in Great Mosquito Cove and Bull Arm

Model Site	Longitude (°W)	Latitude (°N)	Approximate Bottom Depth (m)	Model Scenarios
Casting basin wall	53.8859	47.8101	12	Sheet pile driving, vessel traffic
Drydock exit	53.8853	47.8091	12	Blasting
Deepwater site	53.8665	47.8242	130	Pile driving, vessel traffic

4.2 Bathymetry and Acoustic Environment

4.2.1 Bathymetry

The relief of the sea floor is an important parameter affecting the propagation of underwater sound, and detailed bathymetric data are therefore essential to accurate modeling. A base-level-resolution bathymetric dataset for the entire study area was obtained from the SRTM30_Plus public domain digital terrain model (DTM) (Becker and Sandwell, 2008). This DTM, currently at version 4.0, is based on a combination of satellite-based synthetic aperture radar altimetry and vessel-based bathymetric measurements. The horizontal grid resolution is 30 arc-seconds; for the current study area, this corresponds to one depth/elevation estimate approximately every 900 m in the north-south direction and every 600 m in the east/west direction. This base-level grid was sub-sampled at 10 m resolution to create a base-level 10 m Digital Terrain Model (DTM).

This base-level DTM was augmented with two more localized, higher-resolution bathymetric datasets. Bathymetric data for Bull Arm north of latitude 47° 47' were obtained by digitizing Canadian Hydrographic Service chart #4851 (scale of 1:60,000) using a square grid with a horizontal resolution of 100 m. The result was sub-sampled in the same way as the base-level grid and merged with it, over-riding the base-level grid in areas where the two overlapped. Finally, higher-resolution bathymetric data were derived for the inshore half of Great Mosquito Cove by digitizing a bathymetric contour map

presented by NGL (1990). The resulting data were gridded and integrated into the 10 m resolution modeling DTM using the same procedure. Bathymetric contours generated from the resulting DTM data are plotted in Figure 7.

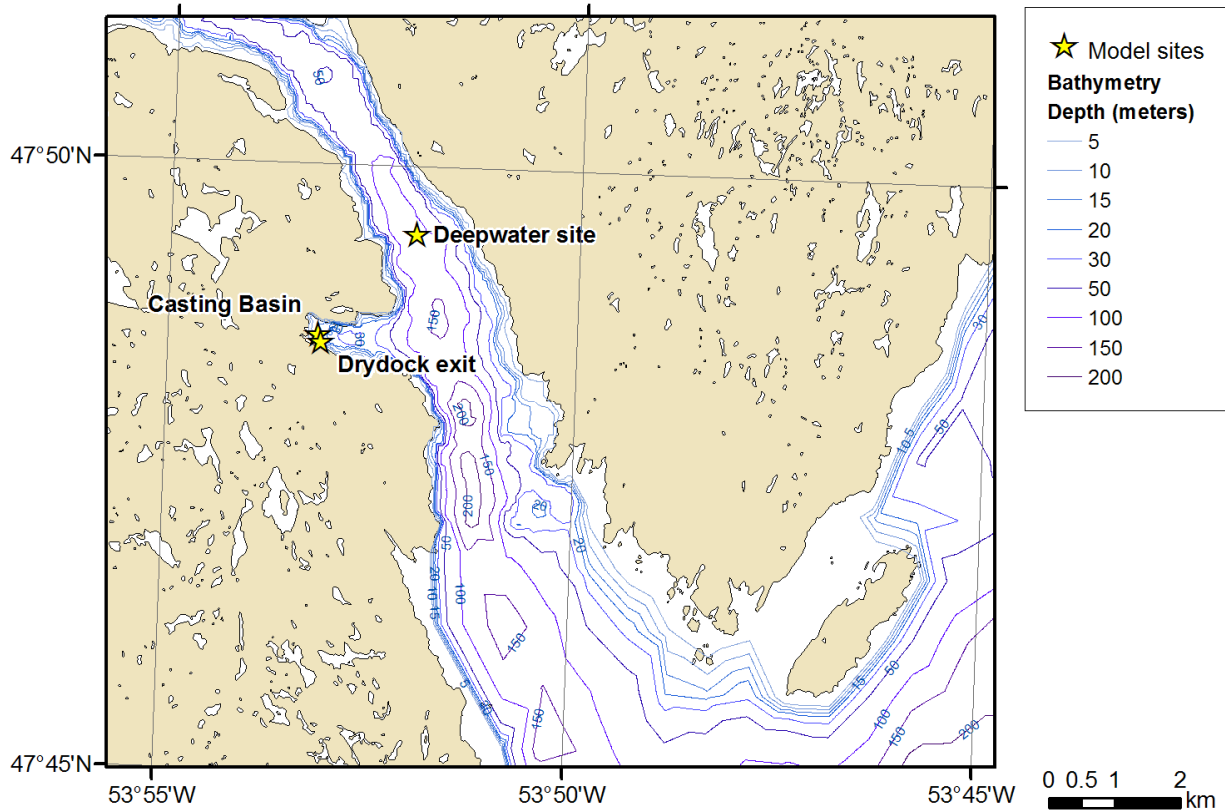


Figure 7: Model sites and depth contours for the Bull Arm model area

4.2.2 Geoacoustic Properties

The area inside Great Mosquito Cove was relatively well surveyed following construction of the Hibernia GBS and subsequent removal of the dry-dock berm, using surficial sediment sampling and video survey techniques (Lee, 2005). The predominant sediment type is sand, often with gravel content. The frequent outcrops of consolidated sediments (Lee, 2005) suggest a very thin layer of unconsolidated sediments on top of the bedrock.

Seabed geoacoustic parameters for the unconsolidated sediment cover in Great Mosquito Cove were estimated using Buckingham’s sediment grain-shearing model (Buckingham, 2005), which computes the acoustic properties of the sediments from porosity and grain-size measurements or estimates. The geoacoustic profile was estimated assuming medium sand with 65% porosity; the latter value was selected based on a generic porosity curve (Einsele, 2000). Based on the frequent outcrops of bedrock observed by Lee (2005), the average thickness of the layer of unconsolidated sediments was estimated to be small, at 5 m. According to NGL (1989), the bedrock around Mosquito Cove is represented by siltstones and sandstones. Average geoacoustic parameters for these rock types were chosen based on values presented by Barton (2006). The resulting depth-dependent estimates of density (ρ), compressional speed (V_p), compressional attenuation coefficient (α_p), shear wave speed (V_s), and shear wave attenuation coefficient (α_s) are shown in Table 3 below.

Table 3: Geoacoustic model for the Great Mosquito Cove area

depth (mbsf ^a)	ρ (g/cm ³)	V_P (m/s)	α_P (dB/ λ)	V_S (m/s)	α_S (dB/ λ)
0–5	1.61	1540–1730	0.3–1.0	200	0.2
>5	2.7	3000	0.05		

^a mbsf = meters below sea floor

The available sediment samples for the portion of Bull Arm adjacent to Great Mosquito Cove suggest coarser content for the surficial sediments (Davidson, 1990). It was assumed that the predominant sediment type for Bull Arm is sandy gravel with 60% porosity. The overall thickness of the surficial sediment layer and the properties of the underlying bedrock were assumed to be the same as in Great Mosquito Cove. The resulting geoacoustic model for Bull Arm area is presented in Table 4.

Table 4: Geoacoustic model for the Bull Arm area

depth (mbsf ^a)	ρ (g/cm ³)	V_P (m/s)	α_P (dB/ λ)	V_S (m/s)	α_S (dB/ λ)
0–5	1.7	1660–2200	0.7–2.0	250	0.5
>5	2.7	3000	0.05		

^a mbsf = meters below sea floor

4.2.3 Sound Speed Profiles

Water column sound speed profiles (SSPs) for the survey area were computed from temperature and salinity profiles downloaded from the U.S. Naval Oceanographic Office’s Generalized Digital Environmental Model (GDEM) database (Teague *et al.* 1990). The latest release of the GDEM database (version 3.0) provides average monthly profiles of temperature and salinity for the world’s oceans on a latitude-longitude grid with 0.25-degree resolution. Profiles in GDEM are provided at 78 fixed depth points up to a maximum depth of 6800 m. The profiles in GDEM are based on historical observations of global temperature and salinity from the U.S. Navy’s Master Oceanographic Observational Data Set (MOODS). GDEM provides historical average profiles that extend to the deepest depth in a given 15-arc-minute square.

Temperature-salinity profiles from GDEM were converted to sound-speed profiles (SSPs) using the equations of Coppens (1981):

$$c(z, T, S) = 1449.05 + 45.7T - 5.21t^2 - 0.23t^3$$

$$+ (1.333 - 0.126t + 0.009t^2)(S - 35) + \Delta$$

$$\Delta = 16.3Z + 0.18Z^2$$

$$Z = (z/1000)(1 - 0.0026 \cos(2\phi))$$

$$t = T/10$$

Here z is depth in meters, T is temperature in degrees Celsius, S is salinity in psu, and ϕ is latitude (in radians).

Construction activities in Bull Arm and Great Mosquito Cove may occur year-round. In order to generate precautionary estimates of the underwater sound field, the “worst-case” sound speed profile (i.e., most favorable to long-range sound propagation) was used for sound propagation modeling. As shown in

Figure 8, the February SSP for SW Trinity Bay generally allows the source to ensonify more of the study area than those for other times of the year. The February SSP is slightly upward-refracting, a condition which reduces bottom loss. This can be contrasted with the month of August, for example, which is strongly downward-refracting, causing more of the sound energy ultimately to be directed into the sediment layers, where it would be attenuated. The other months exhibit SSPs that have characteristics between these two extremes. A plot of the actual February SSP used in the modeling is shown in Figure 9, along with the corresponding September profile for comparison.

Although the available GDEM data correspond to sites in SW Trinity Bay, there are a few individual SSP profiles available from NODC for the lower half of Bull Arm. A comparison was made between these individual profiles and the statistical average profiles from GDEM, and a very good correspondence was found.

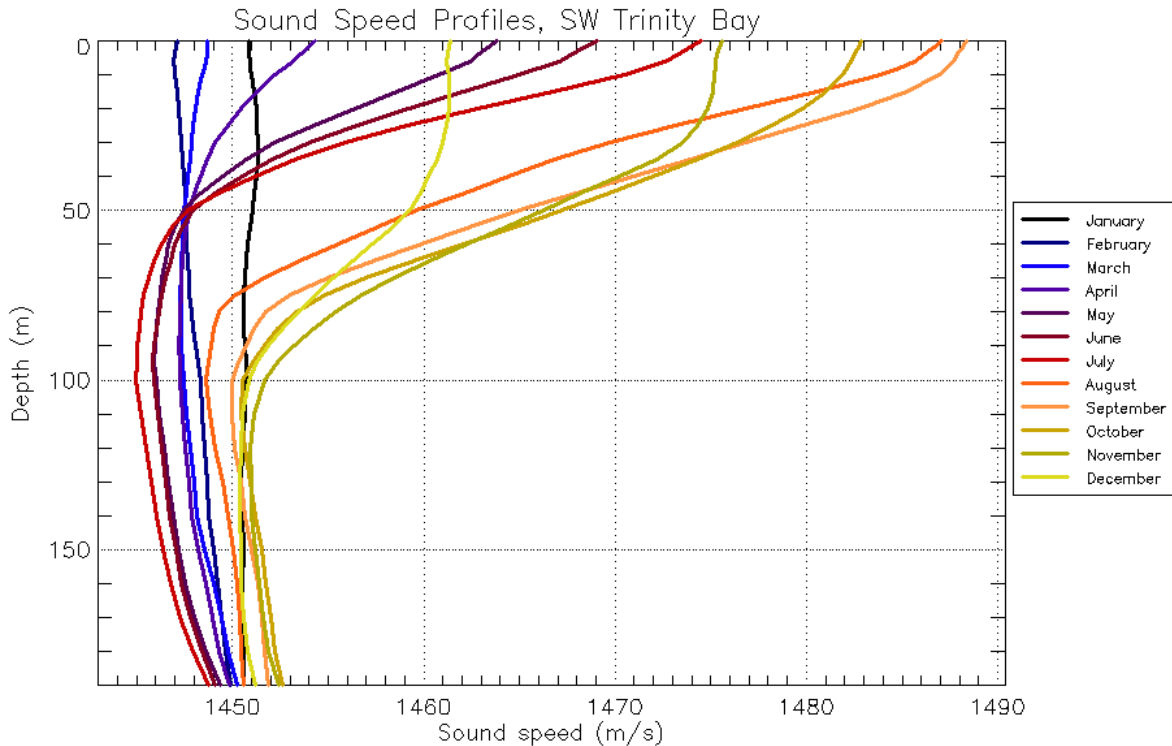


Figure 8: Typical monthly sound speed profiles in SW Trinity Bay, based on GDEM

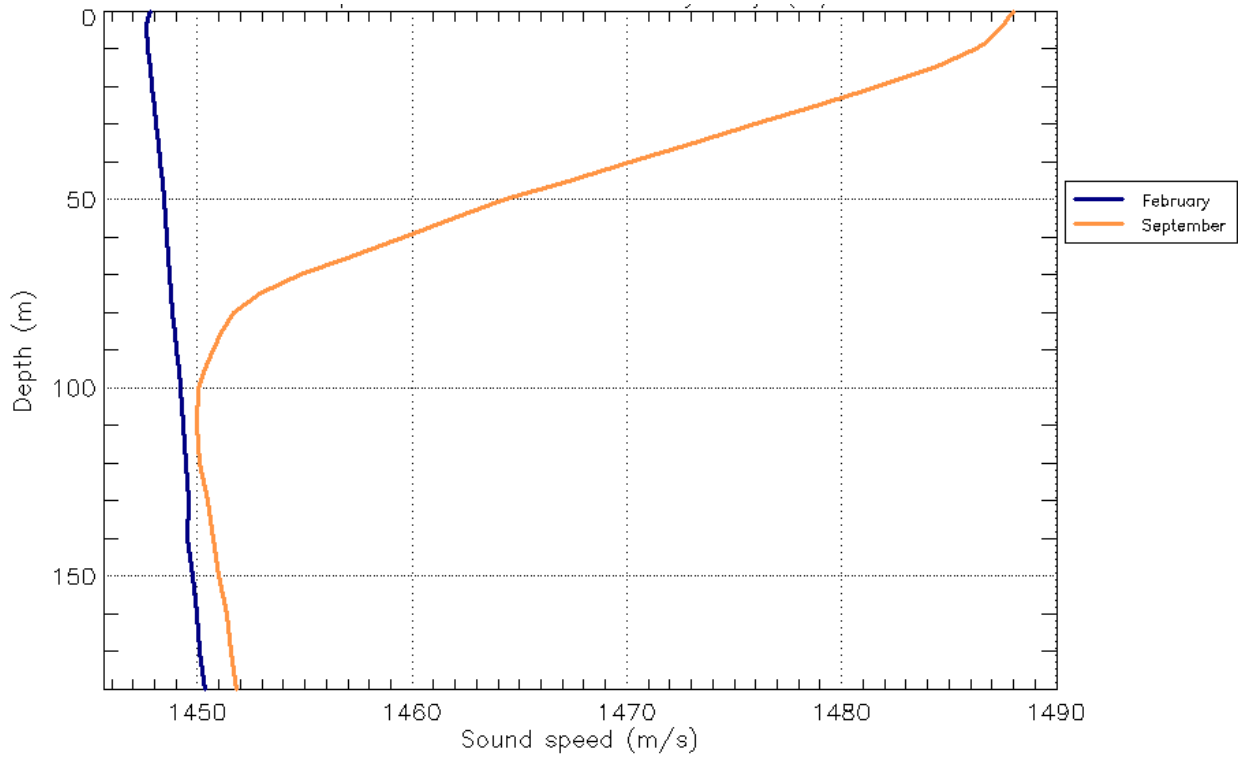


Figure 9: Average February and September sound speed profiles at 47.75°N, 53.75°W, based on GDEM

5 Model Results

The MONM sound propagation model was run in the full $n \times 2-D$ sense as described in Section 3.1 for the model scenarios, source levels, and environmental parameterization described in Sections 2 and 4. Geographically-rendered maps of the sound pressure level are shown in the figures of the sub-sections below. The level depicted at each location is the maximum predicted level for that location at any depth down to the bottom. Note that the SPL for the two impulsive sources (impact hammering and blasting) has been estimated from the SEL as discussed in Section 3.2.1, assuming a pulse length of 100 ms; i.e., estimated SPL is obtained by adding 10 dB to the SEL.

The tables in the following sub-sections summarize the results of the acoustic modeling in terms of radii to specified threshold levels between 120 and 190 dB re 1 μ Pa SPL over all modeled depth strata down to the sea floor. Radii are presented both without frequency weighting and for M-weightings corresponding to low-, mid-, and high-frequency cetaceans and to pinnipeds in water (see Section 3.2.2). Radii shown are 95th percentile radii. Given a regularly gridded spatial distribution of modeled received levels, the 95th percentile radius is defined as the radius of a circle that encompasses 95% of the grid points with received levels equal to or greater than the threshold value. Note that the radial resolution of the model runs was 10 m.

5.1 Impact Hammering

Radii are shown in Table 5 and Table 6 for impact hammering at the casting basin wall and at the deepwater site, respectively. As discussed in Section 2, the same source levels were used for both scenarios, but with different source depths in order to reflect the different nature of the pile driving at the two sites.

The 95th percentile radii for the un-weighted 180 dB re 1 μ Pa level extend to a range of 260 m and 150 m at the casting basin and deepwater sites, respectively. The 120 dB re 1 μ Pa contour extends to or beyond the nearest coastlines in all directions for both sites (Figure 10). In the case of the casting basin site, there is considerable propagation of sound through the sea bottom (e.g., through Big Mosquito Point), so that the 120 dB contour extends some distance up and down Bull Arm (Figure 10, upper panel).

Application of M-weightings for mid-frequency and high-frequency cetaceans reduces the radii for SPL contours not bounded by topography, although the reduction is not great, as much of the energy of the impact hammer occurs at intermediate frequencies (Figure 2, Section 2.1). Note that the slight increase in the 120 dB re 1 μ Pa radius shown for M_{lf} weighting in the top row of Table 5 is a result of reduction of the up- and down-Arm “lobes” mentioned in the above paragraph (Figure 10, upper panel), which biases the 95th percentile upward slightly. As the 120 dB re 1 μ Pa contour is bounded by the walls of Great Mosquito Cove and Bull Arm for all weightings, this is not a significant difference.

Table 5: Estimated 95th percentile radii for impact hammering at the casting basin wall in Great Mosquito Cove

Estimated SPL (dB re 1 μ Pa)	SEL (dB re 1 μ Pa ² ·s)	95 th percentile radius (km)				
		Un-weighted	M _{if}	M _{mf}	M _{hf}	M _{pw}
120	110	3.5	3.5	3.5	3.6	3.5
130	120	3.6	3.6	3.6	3.6	3.6
140	130	3.6	3.6	3.5	3.5	3.6
150	140	3.3	3.3	3.2	3.2	3.3
160	150	2.9	2.9	1.6	1.3	2.8
170	160	0.99	0.99	0.65	0.52	0.89
180	170	0.26	0.26	0.16	0.13	0.22
190	180	0.06	0.06	0.02	0.02	0.05

Table 6: Estimated 95th percentile radii for impact hammering at the deepwater site in Bull Arm

Estimated SPL (dB re 1 μ Pa)	SEL (dB re 1 μ Pa ² ·s)	95 th percentile radius (km)				
		Un-weighted	M _{if}	M _{mf}	M _{hf}	M _{pw}
120	110	21.6	21.6	21.6	21.6	21.6
130	120	21.3	21.3	21.2	21.2	21.3
140	130	20.3	20.3	18.4	15.0	19.9
150	140	9.0	8.8	6.6	5.0	7.9
160	150	3.1	3.0	2.0	1.8	2.4
170	160	0.83	0.82	0.49	0.36	0.67
180	170	0.15	0.15	0.07	0.06	0.12
190	180	0.02	0.02	0.01	0.01	0.02

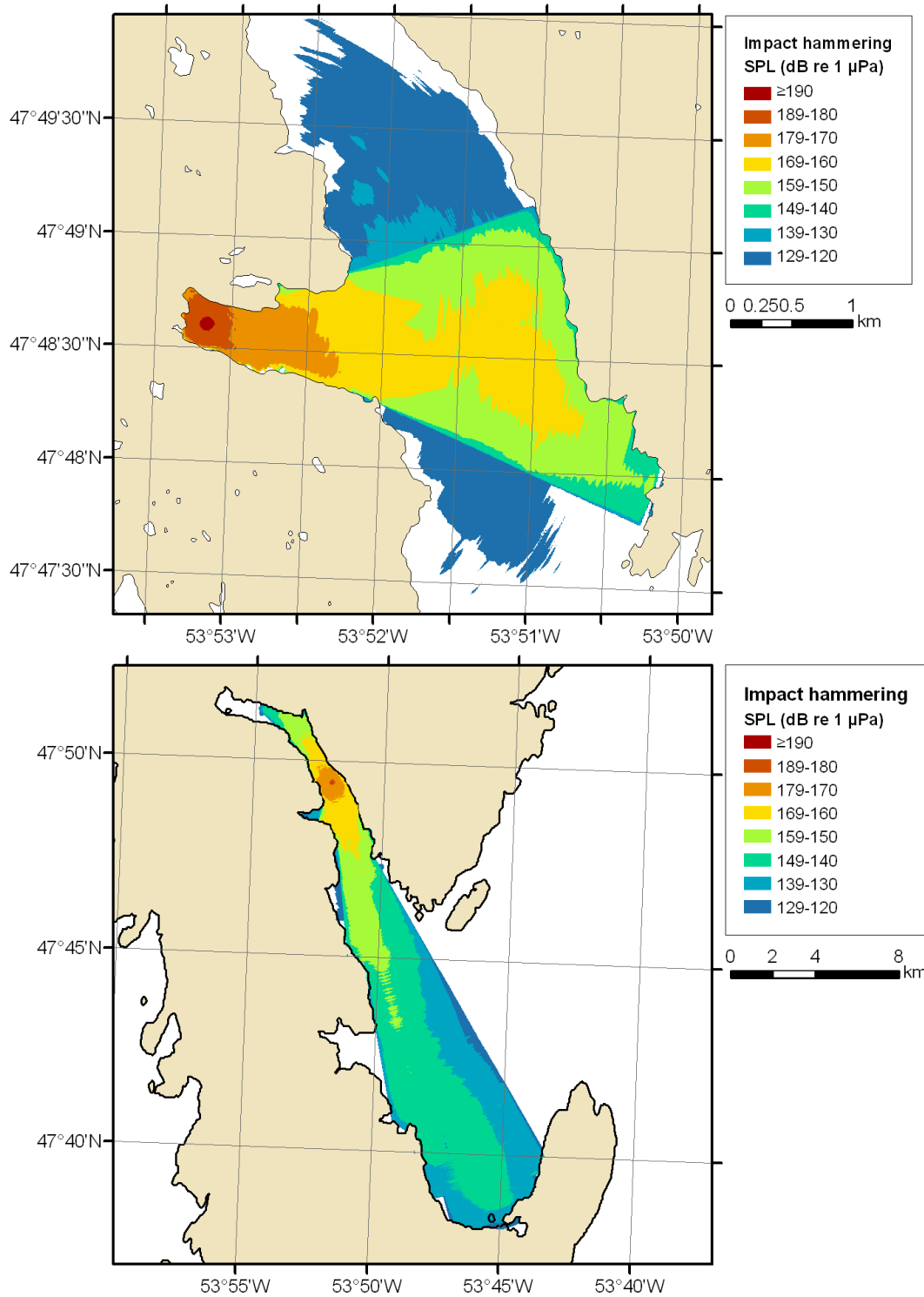


Figure 10: Estimated un-weighted, single-blow sound pressure level for operation of an impact hammer at the casting basin wall in Great Mosquito Cove (top panel) and at the deepwater site (bottom panel). Modeled source depth is 6 m above the sea floor in both cases.

5.1.1 Cumulative SEL

Based on a review of available literature on marine mammal hearing and on physiological (and behavioral) responses to anthropogenic sound, Southall *et al.* (2007) have recently proposed alternative criteria for auditory injury in marine mammals, based on the peak pressure and sound exposure level metrics. These take into account the type of sound (non-pulse, single-pulse, or multiple-pulse), as well as the broad hearing capabilities of the mammals involved. For a multiple-pulse source such as an impact hammer, an SEL-based injury criterion of 198 dB re 1 $\mu\text{Pa}^2\cdot\text{s}$ (M-weighted) is proposed for cetaceans. The corresponding level for pinnipeds in water is 186 dB re 1 $\mu\text{Pa}^2\cdot\text{s}$. The SEL is summed over multiple pulse exposures as described in Section 3.2, based on the precautionary assumption that there is no recovery of hearing between exposures.

In the case of a stationary source and receiver it is fairly straightforward to estimate the cumulative SEL (CSEL) over a given period of time. As each pulse is identical to the last and no hearing recovery occurs between pulses, the CSEL is simply a multiple of the single-pulse SEL:

$$\text{CSEL} = 10 \log_{10} \left\{ \frac{\sum_{n=1}^N \int_0^T p_n^2(t) dt}{p_{ref}^2} \right\} = \text{SEL} + 10 \log_{10} N,$$

where N is the number of pulses summed. Southall *et al.* (2007) do not clearly specify an integration period, so that the CSEL is highly sensitive both to the nature of the activity and to the integration period.

To illustrate this, the 198 dB re 1 $\mu\text{Pa}^2\cdot\text{s}$ CSEL contour is plotted in Figure 11 for two M-weightings (low-frequency and high-frequency cetaceans), and for integration periods ranging from 1 minute to 1 day. The CSEL was computed based on a blow rate of 32 blows/minute (Menck GmbH, 2009). The maximum CSEL was selected over all receiver depths, representing the worst-case situation in which an animal is present at a fixed location and depth (the depth of maximum ensonification) throughout the integration period. Depending on the integration period selected, the Southall *et al.* (2007) CSEL criterion is achieved over a varying portion of Great Mosquito Cove, and extending into Bull Arm for low-frequency cetaceans and a 24 h integration period (Figure 11).

Southall *et al.* (2007) also indicate that, in cetaceans, auditory injury may occur upon exposure to a (flat-weighted) peak pressure of ≥ 230 dB re 1 μPa . The criterion for pinnipeds in water is 218 dB re 1 μPa . While the range-dependent peak pressure was not computed in this study (this requires a full-waveform model; see Section 3.2.1), Greene and Davis (1999) reported peak pressure levels of 180 dB re 1 μPa for a receiver at a range of 1.5 km from the source and a depth of 18 m. For another relatively large impact hammer (Delmag D62-22, with maximum impact energy of 223 kJ), Blackwell (2005) reported a peak pressure 206 dB re 1 μPa at a range of 62 m. Based on these values and the CSEL estimates described above, the CSEL criterion is expected to be the more precautionary of the two injury criteria presented by Southall *et al.* (2007).

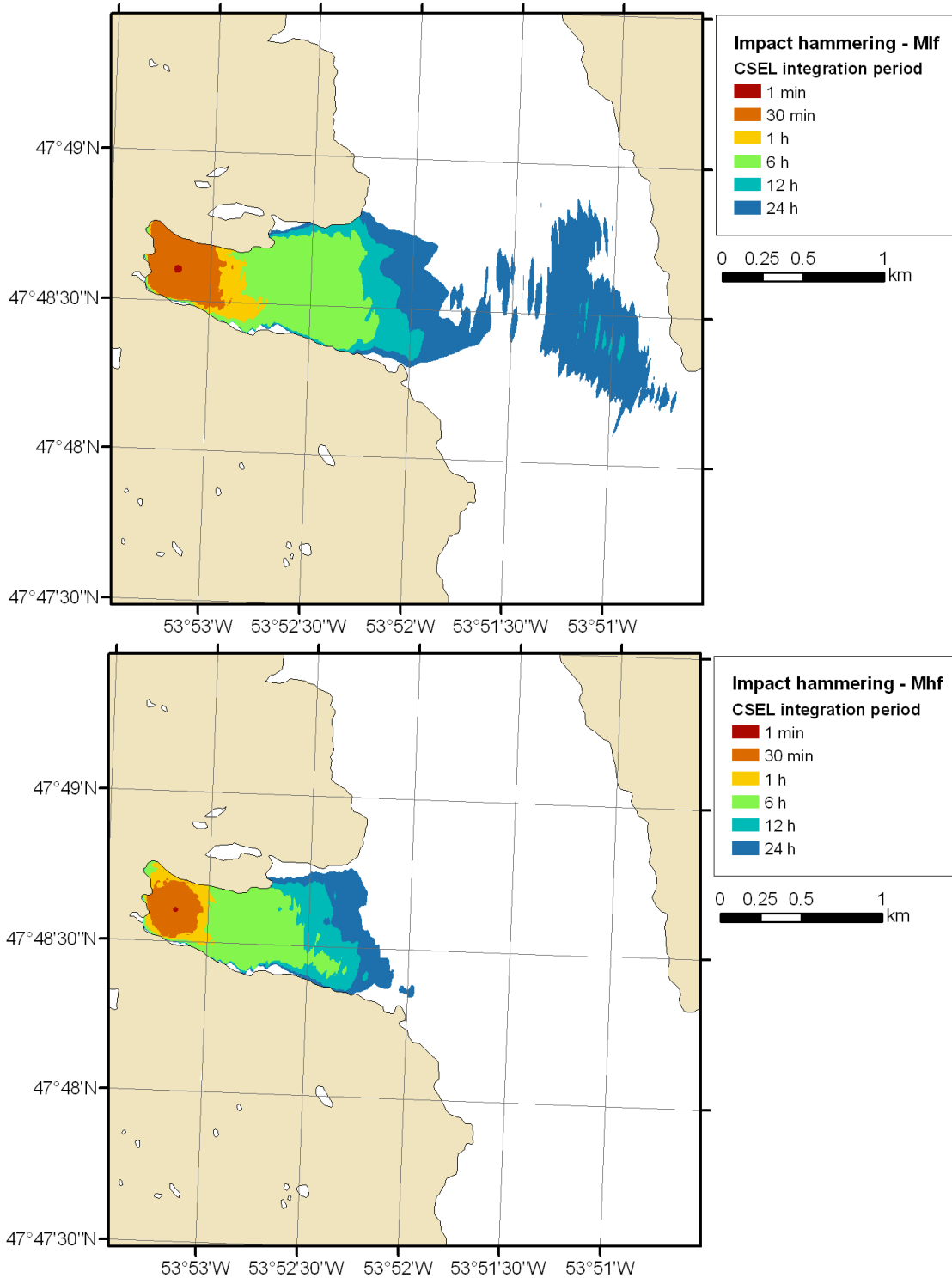


Figure 11: Estimated 198 dB re 1 $\mu\text{Pa}^2\cdot\text{s}$ cumulative SEL contour for impact hammering at the casting basin wall, assuming a blow rate of 32 blows/minute and CSEL integration periods from 1 minute to 24 hours. Contours are shown for low-frequency (top panel) and high-frequency (bottom panel) cetacean M-weightings. Setup otherwise as in the upper panel of Figure 10.

5.2 Vessel Traffic

Radii are shown in Table 7 and Table 8 for operation of a tug at high power levels at the casting basin wall and at the deepwater site, respectively. As expected given the relative source levels (Section 2), 95th percentile radii are much smaller for the tug than for impact hammering. The SPL is below the 180 dB re 1 μ Pa level even one model range step from the vessel, although the 120 dB re 1 μ Pa contour still extends to a maximum range of 16.7 km at the deepwater site (Table 8, Figure 12). As discussed in Section 2.2, radii would be smaller for lower-power activities such as transit. As with impact hammering, application of higher-frequency M-weightings generate a slight reduction in radii.

Table 7: Estimated 95th percentile radii for operation of a tug at the casting basin wall in Great Mosquito Cove

Estimated SPL (dB re 1 μ Pa)	95 th percentile radius (km)				
	Un-weighted	M _{lf}	M _{mf}	M _{hf}	M _{pw}
120	3.5	3.5	3.5	3.5	3.5
130	3.0	3.0	2.9	2.8	3.0
140	1.2	1.2	1.0	0.96	1.1
150	0.46	0.46	0.30	0.26	0.38
160	0.14	0.14	0.09	0.07	0.10
170	0.02	0.02	< 0.01	< 0.01	0.02
180	< 0.01	< 0.01	< 0.01	< 0.01	< 0.01
190	< 0.01	< 0.01	< 0.01	< 0.01	< 0.01

Table 8: Estimated 95th percentile radii for operation of a tug at the deepwater site in Bull Arm

Estimated SPL (dB re 1 μ Pa)	95 th percentile radius (km)				
	Un-weighted	M _{lf}	M _{mf}	M _{hf}	M _{pw}
120	16.7	16.7	14.4	11.2	15.9
130	5.4	5.4	4.1	3.4	4.8
140	1.8	1.8	1.3	1.0	1.7
150	0.42	0.41	0.23	0.20	0.32
160	0.06	0.06	0.04	0.03	0.05
170	0.02	0.02	0.01	0.01	0.02
180	< 0.01	< 0.01	< 0.01	< 0.01	< 0.01
190	< 0.01	< 0.01	< 0.01	< 0.01	< 0.01

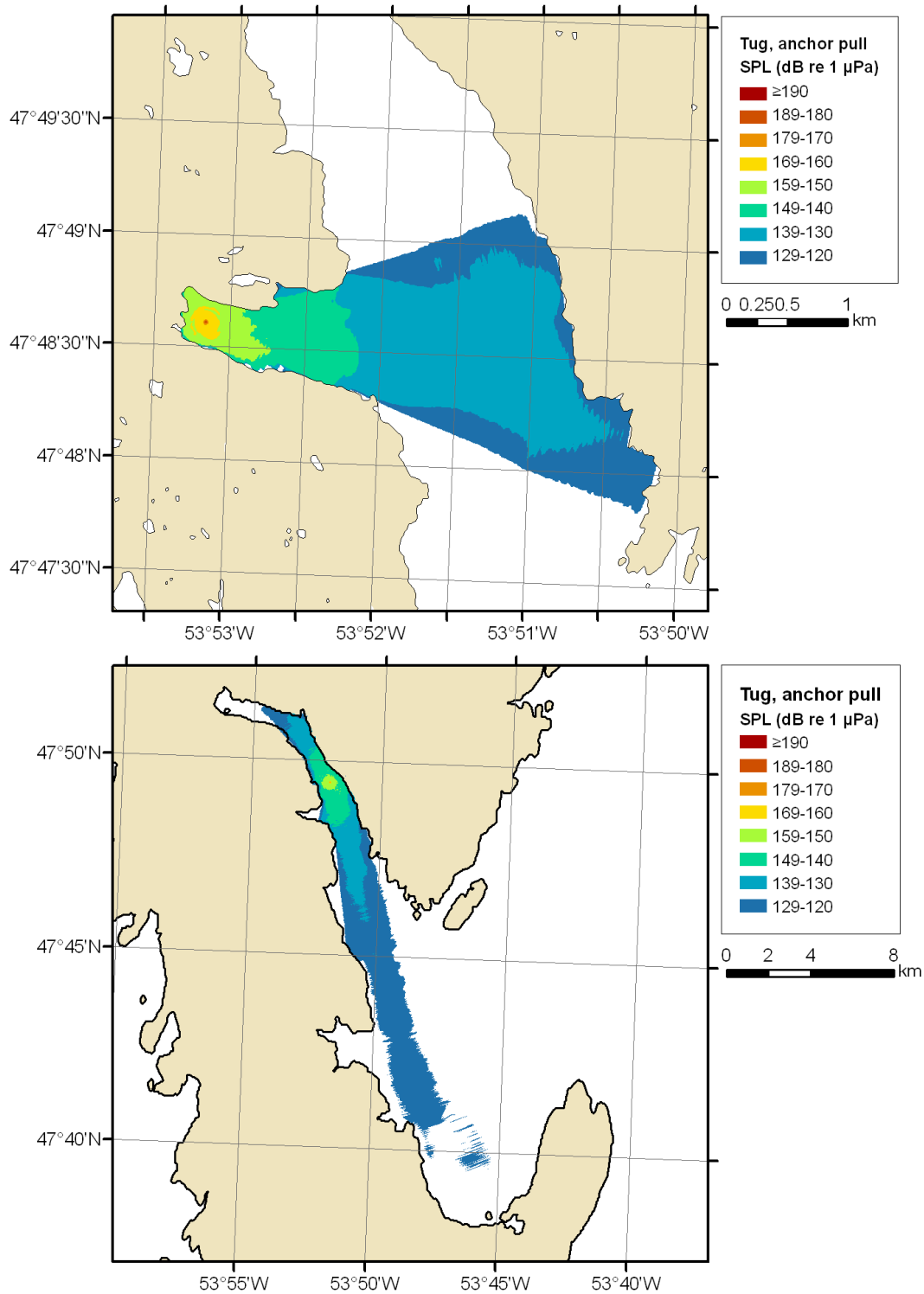


Figure 12: Estimated un-weighted sound pressure level for operation of a tug at the casting basin wall in Great Mosquito Cove (top panel) and at the deepwater site (bottom panel). Source depth is 3 m in both cases.

5.3 Blasting

Radii are shown in Table 9 for blasting in Great Mosquito Cove; the corresponding sound field is mapped in Figure 13. As expected given the source levels presented in Section 2.3, the radii for this activity are greater than those for either impact hammering or operation of a tug. All radii up to and including the 180 dB re 1 μ Pa radius extend to the opposite shoreline for the un-weighted model results. As with the impact hammering scenario, there is significant sound transmission through the sea bottom as well as through the water. Because the peak in the source spectrum occurs at a lower frequency than the two other scenarios described here (Section 2), the reduction in radii associated with the application of M-weightings for mid- and high-frequency cetaceans is more significant (Table 9).

As discussed in Section 2.3, the scenario described below is illustrative of the loudest single charge that is permissible under the DFO 100 kPa overpressure guideline (Wright and Hopky, 1998). In practice, various approaches may be used to reduce the impact for a given overall explosive charge, including sub-dividing a large charge into a series of smaller, time-delayed charges or using additional mitigation measures such as bubble curtains (Wright and Hopky, 1998).

Table 9: Estimated 95th percentile radii for blasting near the exit from the casting basin in Great Mosquito Cove. The 120 dB re 1 μ Pa contour is truncated to the east for the flat and M_{lf} weightings.

Estimated SPL (dB re 1 μ Pa)	SEL (dB re 1 μ Pa ² ·s)	95 th percentile radius (km)				
		Un-weighted	M _{lf}	M _{mf}	M _{hf}	M _{pw}
120	110	>19	>19	18.0	17.1	18.7
130	120	18.7	18.7	7.8	5.4	18.0
140	130	18.0	18.0	3.5	3.3	7.7
150	140	7.8	7.7	3.3	3.3	3.5
160	150	3.5	3.4	3.1	3.1	3.2
170	160	3.0	3.0	2.7	2.6	2.8
180	170	2.7	2.7	0.96	0.92	1.1
190	180	0.99	0.98	0.36	0.35	0.43

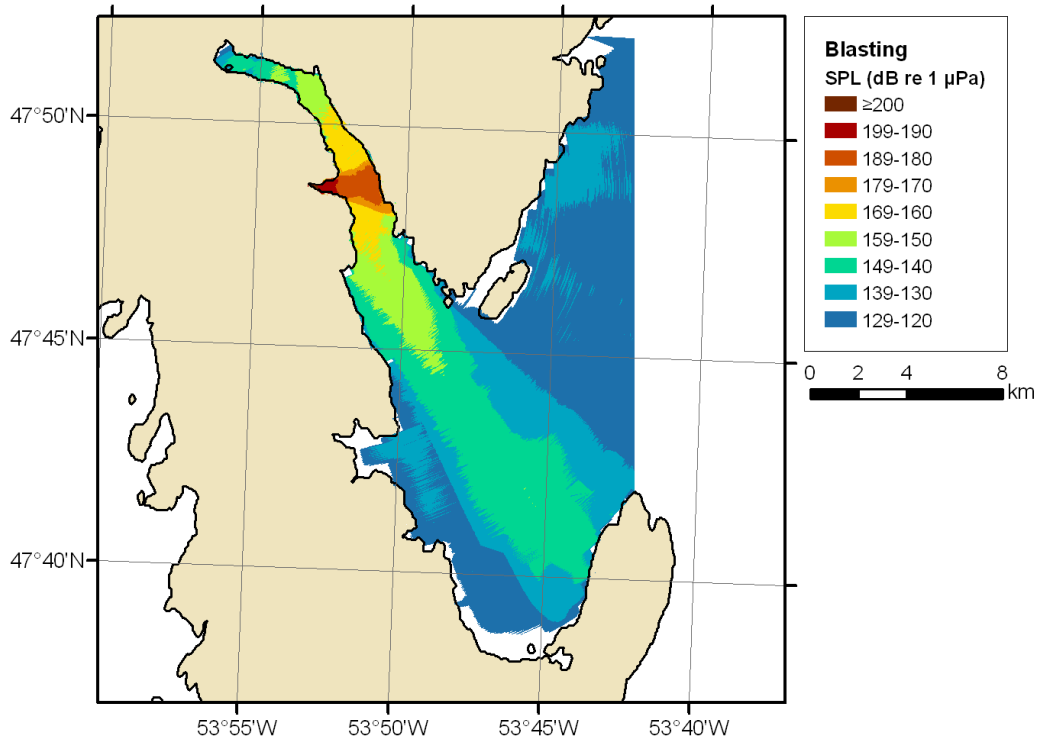


Figure 13: Estimated un-weighted, single-blast sound pressure level for detonation of 2 kg of TNT 7.1 m sub-bottom near the exit from the casting basin in Great Mosquito Cove. The 120 dB re 1 μPa contour is truncated to the east as a result of the model bounds used.

6 References

6.1 Literature Cited

- Austin, M.E., A.O. MacGillivray, D.E. Hannay, and S.A. Carr. *Acoustic monitoring of Marathon Canada Petroleum ULC 2003 Courland/Empire seismic program*. Victoria, British Columbia: JASCO Research Ltd., 2003.
- Barton, N. *Rock Quality, Seismic Velocity, Attenuation and Anisotropy*. Taylor & Francis, 2006.
- Blackwell, S.B. *Underwater measurements of pile-driving sounds during the Port MacKenzie dock modifications, 13-16 August 2004*. Goleta, California: Greeneridge Sciences, Inc., 2005.
- Blackwell, S.B., R.G. Norman, C.R. Greene Jr., and W.J. Richardson. "Acoustic measurements." *Marine mammal monitoring and mitigation during open water seismic exploration by Shell Offshore Inc. in the Chukchi and Beaufort Seas, July–September 2006: 90-day report*: p. 4-1 to 4-52. Anchorage, Alaska: LGL Alaska Research Associates, Inc., 2007.
- Buckingham, M.J. "Compressional and shear wave properties of marine sediments: Comparisons between theory and data." *Journal of the Acoustical Society of America* 117(1): 137-152, 2005.
- Collins, M.D., R.J. Cederberg, D.B. King, and S.A. Chin-Bing. "Comparison of algorithms for solving parabolic wave equations." *Journal of the Acoustical Society of America* 100(1):178-182, 1996.
- Coppens, A.B. "Simple equations for the speed of sound in Neptunian waters." *Journal of the Acoustical Society of America* 69: 862-863, 1981.
- Davidson, L. *Prediction of sediment dispersion and fuel spill transport in Great Mosquito Cove and Bull Arm*. St. John's, Newfoundland: Seaconsult Ltd., 1990.
- Einsele, G. *Sedimentary basins; evolution, facies, and sediment budget (2 ed.)*. Springer, 2000.
- Greene, C.R., Jr. "Physical acoustics measurements." In: W.J. Richardson (ed.). *Northstar marine mammal monitoring program, 1996: marine mammal and acoustical monitoring of a seismic program in the Alaskan Beaufort Sea*: p. 3-1 to 3-63. King City, Ontario: LGL Ltd., 1997.
- Greene, C.R., Jr., and R.A. Davis. *Piledriving and vessel sound measurements during installation of a gas production platform near Sable Island, Nova Scotia, during March and April, 1998*. Santa Barbara, California: Greeneridge Sciences Inc, 1999.
- Hannay, D., A. MacGillivray, M. Laurinolli and R. Racca. *Source Level Measurements from 2004 Acoustics Program*. Victoria, British Columbia: JASCO Research Ltd., 2004.
- Hyde D.W. *Conventional weapons effects computer program, US Waterways Experiment Station Instructional Report SL-88-1*. U.S.A.: U.S. Army Corps of Engineers, 1992.
- Lee, E. *Monitoring Of A Dredged Disposal Site Great Mosquito Cove, Newfoundland. Final Report*. St. John's, Newfoundland: AMEC Earth & Environmental Limited, 2005.
- MacGillivray, A.O., M.M. Zykov, and D.E. Hannay. "Summary of noise assessment." *Marine mammal monitoring and mitigation during open water seismic exploration by ConocoPhillips Alaska, Inc. in the Chukchi Sea, July–October 2006*: p. 3-1 to 3-21. Anchorage, Alaska: LGL Alaska Research Associates, Inc., 2007.
- Malme, C.I., C.R. Greene, and R. A. Davis. *Comparison of radiated noise from pile driving operations with predictions using the RAM model*. King City, Ontario: LGL Ltd., Environmental Research Associates, 1998.
- Malme, C.I., P.W. Smith, and P.R. Miles. *Characterisation of geophysical acoustic survey sounds*. Cambridge: BBN Laboratories, Inc., 1986.

- McCauley, R.D., M.-N. Jenner, C. Jenner, K.A. McCabe, and J. Murdoch. “The response of humpback whales (*Megaptera novaeangliae*) to offshore seismic survey noise: preliminary results of observations about a working seismic vessel and experimental exposures.” *APPEA Journal* 38:692-707, 1998.
- McCauley, R.D., J. Fewtrell, A.J. Duncan, C. Jenner, M.-N. Jenner, J.D. Penrose, R.I.T. Prince, A. Adhitya, J. Murdoch, and K. McCabe. “Marine seismic surveys—a study of environmental implications.” *APPEA Journal* 40:692-708, 2000.
- Miller, J.H., A.E. Bowles, B.L. Southall, R.L. Gentry, W.T. Ellison, J.J. Finneran, C.R. Greene Jr., D. Kastak, D.R. Ketten, P.L. Tyack, P.E. Nachtigall, W.J. Richardson, and J.A. Thomas. “Strategies for weighting exposure in the development of acoustic criteria for marine mammals.” *Journal of the Acoustical Society of America* 118: 2019 (Abstract), 2005. Presentation available at URL: http://www.oce.uri.edu/faculty_pages/miller/Noise_Weighting_10_18_2005.ppt.
- NGL. *Preliminary Study Bull Arm. Final Report*. Newfoundland Geosciences Limited, 1989.
- NGL. “Water and Sediment Parameter Data.” *Analysis of environmental parameters from proposed GBS Construction Area, Great Mosquito Cove and Bull Arm, Trinity Bay, Newfoundland*. St. John’s, Newfoundland: Newfoundland Geosciences Limited, 1990.
- Southall, B.L., A.E. Bowles, W.T. Ellison, J.J. Finneran, R.L. Gentry, C.R. Greene, Jr., D. Kastak, D.R. Ketten, J.H. Miller, P.E. Nachtigall, W.J. Richardson, J.A. Thomas, and P.L. Tyack. “Marine mammal noise exposure criteria: initial scientific recommendations.” *Aquatic Mammals* 33:411-521, 2007.
- Teague, W.J., M.J. Carron, and P.J. Hogan. “A comparison between the generalized digital environmental model and Levitus climatologies.” *Journal of Geophysical Research* 95(C5): 7167-7183, 1990.
- Wright, D.G. and G.E. Hopky. “Guidelines for the use of explosives in or near Canadian fisheries waters”. *Canadian Technical Report of Fisheries and Aquatic Sciences* 2107, 1998.
- Zhang, Z. and C. Tindle. “Improved equivalent fluid approximations for a low shear speed ocean bottom.” *Journal of the Acoustical Society of America* 98:3391-3396, 1995.

6.2 Internet Sites

- Becker, J.J., and D.T. Sandwell. *SRTM30_Plus digital terrain model (DTM), v4.0*. La Jolla, California: Scripps Institution of Oceanography, 2008. Available at URL: http://topex.ucsd.edu/WWW_html/srtm30_plus.html.
- Britoil Offshore Services Website. Singapore: Britoil Offshore Services Pte Ltd., 2007. Available at URL: <http://www.britoil.com.sg/britoil50.htm>.
- Menck GmbH. *MHU Facts and Figures*. Kaltenkirchen, Germany: Menck GmbH, 2009. Available at URL: http://www.menck.com/fileadmin/user_upload/MHU_facts_figures.pdf.